Journal of Alloys and Compounds 519 (2012) 41–46

Contents lists available at SciVerse ScienceDirect

Journal of Alloys and Compounds

journal homepage: www.elsevier.com/locate/jallcom

Structure and magnetic characteristics of Si-doped AlN films

D. Pan[a,b], J.K. Jian[a], Y.F. Sun[a], R. Wu[a,*]

[a] Department of Physics, Xinjiang University, Urumchi 830046, Xinjiang, People's Republic of China
[b] State Key Laboratory for Superlattices and Microstructures, Institute of Semiconductors, Chinese Academy of Sciences, P.O. Box 912, Beijing 100083, People's Republic of China

ARTICLE INFO

Article history:
Received 7 September 2011
Received in revised form 2 December 2011
Accepted 6 December 2011
Available online 16 December 2011

Keywords:
Magnetically ordered materials
Si-doped AlN
Radio frequency reactive sputtering
Crystal structure
Room-temperature ferromagnetism

ABSTRACT

We report on the structural and magnetic properties of $Al_{1-x}Si_xN$ films with $0 \leq x \leq 0.11$ deposited on Si (1 0 0) substrates by radio frequency reactive sputtering. X-ray diffractometry (XRD) and energy-dispersive X-ray spectroscopy (EDS) analysis clearly showed that Si atoms were successfully incorporated into AlN, while the crystal structure of the films was maintained. The magnetization curves indicated all the Si-doped AlN films exhibited room-temperature ferromagnetism. Ferromagnetism signals of Si-doped AlN enhanced with increasing Si content and the maximum saturation magnetization (M_s) and coercive field (H_c) obtained at 300 K were about 3.13×10^{-6} emu and 110 Oe, respectively. The results reveal that Si is a potential nonmagnetic dopant for preparing diluted magnetic semiconductor films. It is speculated that the defects-related effects play an important role to determine the long-range magnetic order in Si-doped AlN.

1. Introduction

Diluted magnetic semiconductors (DMSs) have attracted considerable attentions owing to their potential applications in spintronics [1]. AlN-based DMSs have been extensively studied by several groups [2–4]. Magnetic transition metal atoms such as Cr, Mn, Fe, Co and Ni are frequently used to fabricate AlN DMSs and ferromagnetism at or above room temperature (RT) has been frequently observed [2,5–8]. However, no convincing evidence could verify the ferromagnetism of the TMs-doped AlN arises from the magnetic ions actually substituting in the lattice. The magnetic elements doping usually suffers from the problems of the precipitates or secondary phase formation. In some TMs-doped AlN, high temperature ferromagnetism is proved from the nanoscale regions consisting of highly concentrated magnetic constituents [6]. Thus, the origin of ferromagnetism in a DMS is difficult to identify when magnetic transition atoms are used as dopants.

On the other hand, there has been increasing evidence that traditional magnetic elements are not the sole source in inducing intrinsic magnetism; Recently, theoretical studies revealed that Mg, Ti and C are promising nonmagnetic elements for preparing AlN DMSs [9–11]. Since such dopants are intrinsically nonmagnetic, their precipitates do not contribute to ferromagnetism. Thus, the observation of ferromagnetism in a DMS with such dopants will certainly classify such a material as an unambiguous DMS. Very recently, several groups have reported the ferromagnetism of the intrinsic nonmagnetic elements doped AlN, such as Cu and Sc [12,13]. Si is also such a dopant and several groups have demonstrated n-type conductivity in AlN by Si doping, doping causes crystal imperfections which can affect the structural and optical properties of the film [14,15]. However, the investigation on the impact of Si incorporation on structural and magnetic properties is limited. In this paper, the structure, morphology, optical and magnetic properties of Si-doped AlN films with various Si concentrations have been studied. RT ferromagnetic properties of Si-doped AlN films are reported, which shows that the deposited films have potential applications in magneto-electrical devices operating at RT.

2. Experimental

$Al_{1-x}Si_xN$ films, with x varying from 0 to 0.11, were grown on Si (1 0 0) substrates by radio frequency reactive sputtering. The composite target included a high purity (5 N) aluminum target with a diameter of 80 mm and a number of rectangular Si (4 N) pieces 1 mm × 10 mm, which were placed symmetrically on the surface of the Al target for in situ doping. The base pressure in the chamber was below 2×10^{-4} Pa. The deposition conditions for $Al_{1-x}Si_xN$ films were optimized and fixed as follows: the sputtering pressure of pure N_2 gas was maintained at 1.5 Pa, the sputtering power was 300 W, the substrate temperature during deposition was 370 °C, the substrate-to-target distance was 60 mm and the sputtering time was kept constant at 1 h. The typical thickness of the deposited films was about 600 nm. The Si contents were controlled by varying the number of Si pieces.

X-ray diffraction (XRD, Rigaku D/Max-A, Cu $K\alpha$) techniques were used to study the structural properties of the films. Energy dispersive X-ray spectroscopy (EDS) was used to measure the Si concentrations. Because the sampling depth of EDS (0.1–2 μm) is greater than the film thickness, the Si signal from the Si substrate would be included in direct measurements of the Si/Al ratios of the films grown on Si substrate. Therefore, ITO glass substrates were also loaded in the sputtering

* Corresponding author. Tel.: +86 991 8583183; fax: +86 991 8582405.
E-mail address: rongwu1022@163.com (R. Wu).

0925-8388/$ – see front matter © 2011 Elsevier B.V. All rights reserved.
doi:10.1016/j.jallcom.2011.12.015

chamber to simultaneously prepare reference samples. The Si concentrations of the $Al_{1-x}Si_xN$ films on ITO glass substrates were measured, and we assumed that the $Al_{1-x}Si_xN$ films simultaneously grown on Si substrates had the same or similar Si concentrations. The electronic binding energy of Si was determined from X-ray photoemission spectra (XPS, Kratos Amicus, Manchester, U.K.). Surface morphology was investigated by atomic force microscopy (AFM, NT-MDT Slover-P47) in semi-contacting mode and magnetic properties were measured with a superconducting quantum interference device magnetometer (SQUID, MPMS-7) in the temperature range 5–300 K. Photoluminescence (PL) spectra of the samples were measured on a Hitachi F-4500 Fluorescence spectrophotometre at RT excited by the 250 nm line of a Xe lamp as excitation source.

3. Results and discussion

3.1. XRD analysis

Fig. 1 shows the XRD patterns for the AlN films deposited with different Si concentrations. All the films predominantly showed AlN (0 0 2) peaks, implying that films possessed a hexagonal wurtzite structure with a preferred *c*-axis orientation. The incorporation of a small concentration of Si did not affect the preferred orientation. The (0 0 2) peak position shifted to higher angles as *x* increased from 0 to 0.08 (see inset), suggesting the incorporation of Si ions into the AlN matrix and on the substitutional lattice sites as reported in Mn and Si doped AlN films [2,16]. When Si concentration raised to 11%, the (0 0 2) peak slightly moved back to a lower angle and Si (2 1 1) peak appeared in the XRD pattern indicating the generation of Si secondary phase in the film samples and this phenomenon has been found in Cu-doped AlN films [12]. Fig. 2 illustrates the rocking curves of (0 0 2) AlN peak for $Al_{1-x}Si_xN$ (x = 0–0.11) films. It is observed that the full width at half maximum of the (0 0 2) peaks was increased from 9.06° to 13.28° with increasing Si concentration. This revealed that the crystalline property was decreased, which may be due to the Si doping induced defects in the AlN films.

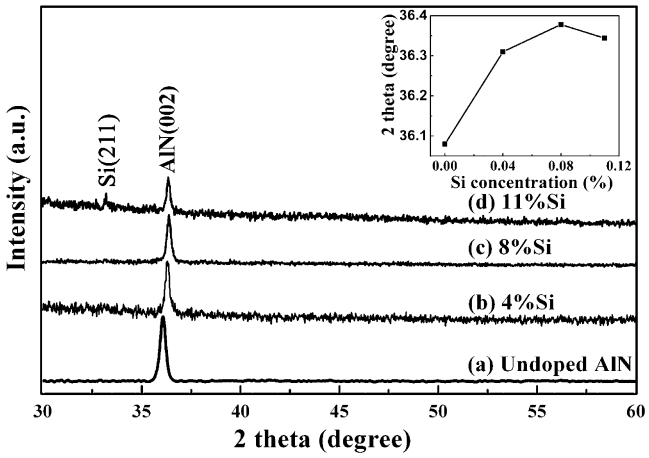

Fig. 1. XRD patterns for the $Al_{1-x}Si_xN$ films with (a) x = 0; (b) x = 0.04; (c) x = 0.08; (d) x = 0.11. The inset shows the variation of (0 0 2) AlN peak position as a function of Si content.

No peaks for Al and other impurities were detected in the measured range.

3.2. AFM analysis

The surface of $Al_{1-x}Si_xN$ films with x = 0, 0.04, 0.08, and 0.11 show root mean square roughness values of 5.0, 8.9, 4.2, and 4.3 nm, respectively, and the morphology changes as shown in Fig. 3. All the deposited film samples possess similar smooth surface and homogeneous grain size. When the Si doping content is larger than 8%, the size of the grains gets small. This morphology

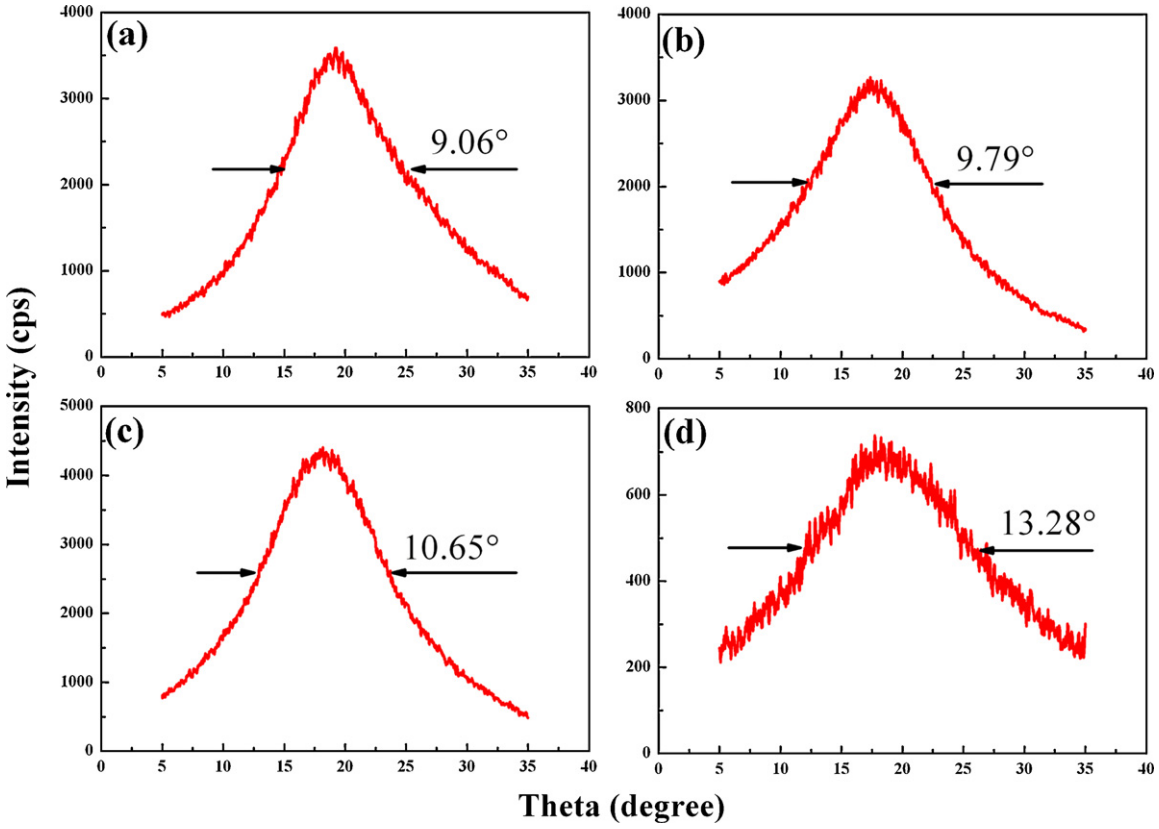

Fig. 2. Rocking curves of (0 0 2) AlN peak for the $Al_{1-x}Si_xN$ films with (a) x = 0; (b) x = 0.04; (c) x = 0.08; (d) x = 0.11.

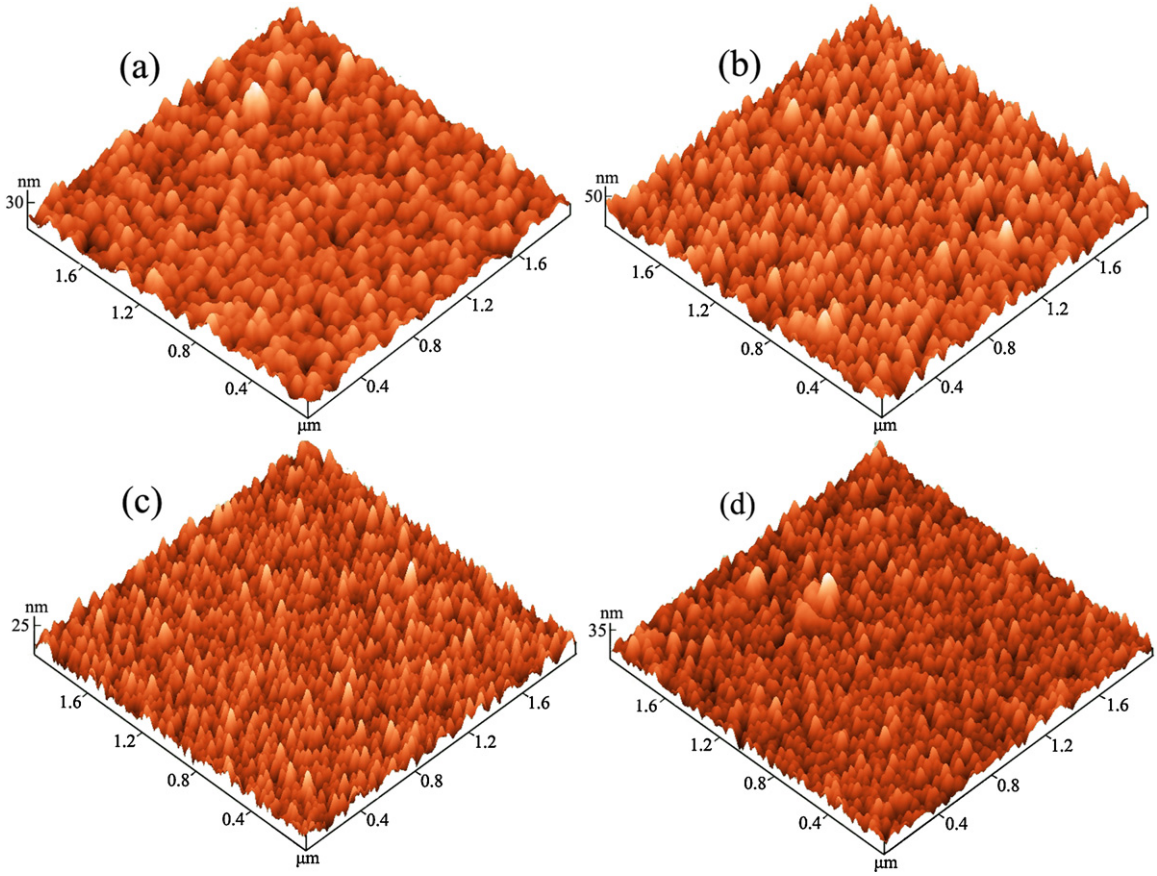

Fig. 3. AFM images for the $Al_{1-x}Si_xN$ films with (a) $x = 0$; (b) $x = 0.04$; (c) $x = 0.08$; (d) $x = 0.11$.

change is consistent with a fact that high Si doping will deteriorate the crystal quality of AlN films.

3.3. Composition analysis

Fig. 4 is a typical EDS spectrum of Si-doped AlN film with $x = 0.08$, which reveals the film is composed of aluminum, nitrogen, and silicon, indicating the existence of Si doping (the signal of oxygen, indium and tin originate from the ITO glass substrate). The inset of Fig. 4 shows an XPS spectrum of Si for the sample ($Al_{0.92}Si_{0.08}$)N on ITO glass substrate. The peak position for the Si $2p_{3/2}$ is 104.40 eV, compared to the value of 99.15 eV and 103.40 eV for pure Si and

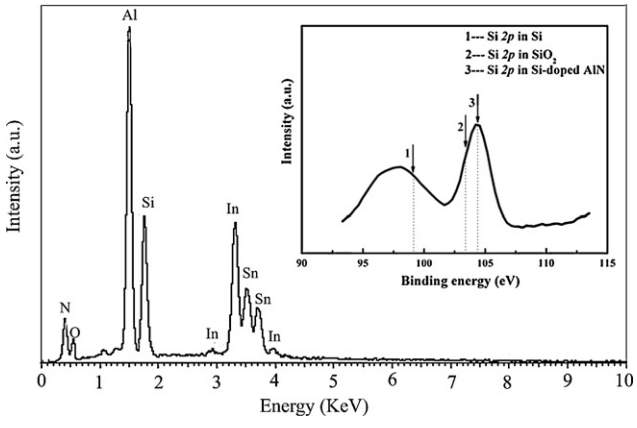

Fig. 4. EDS spectrum of Si-doped AlN film with $x = 0.08$ and the inset shows its XPS spectrum.

SiO_2, respectively [17]. This means that there are no Si and SiO_2 formed in the sample. When Si was doped into AlN films during radio frequency reactive sputtering, Si atoms have two possible formations: (1) complex with Al or N and form AlSi or SiN_x phases; (2) replace Al atoms and subsequent Si—N bond formation. Thus, Si-doped AlN becomes a substitutional solid solution of $Al_{1-x}Si_xN$ ternary alloy. The absence of AlSi or SiN_x phases can be ruled out since they were not detected in this study. Moreover, in Si-doped AlN, possible bonds are Si—N (length: 1.736 Å [18]), Al—Si (2.43 Å [19]), and Si—Si (2.35 Å). Among them, only the Si—N bond is shorter than the Al—N bond (length: 1.8683 Å). Therefore, Si—N bonds are inclined to be replaced by Al—N bonds. From XRD measurement we have found that as the Si concentration increases, AlN (0 0 2) peak shifts towards larger angle at $x = 8\%$ then back at $x = 11\%$, indicating contraction then expansion of the lattice. Because of that the incorporation of embedded Si should either increase or have no effect on the lattice constant, the Si atom should mainly occupy substitutional lattice sites when $x \leq 8\%$, in line with previously reported results [16,20]. This result supports the formation of the substitutional solid solution of $Al_{1-x}Si_xN$ ternary alloy. In our study, the Si concentration is high and we consider Si impurity band is formed below the conduction band as reported in literatures [21,22].

3.4. Photoluminescence properties

As one powerful characterization mean, PL spectrum is often used to investigate the defects information. Fig. 5 shows the RT PL spectra of the deposited $Al_{1-x}Si_xN$ films ($x = 0$–0.11). Due to technical limitations, the maximum excitation energy is 5.9 eV (210 nm) and hence, no information about band-to-band transitions could be extracted in all our samples. As seen in Fig. 5a, no emission peak

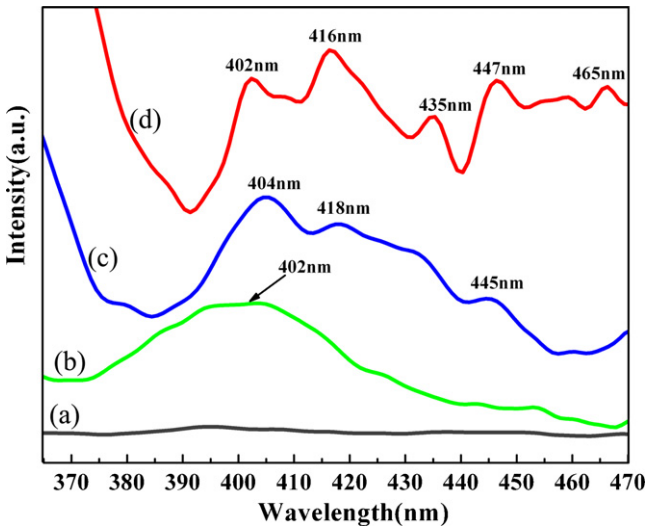

Fig. 5. Photoluminescence spectra of the $Al_{1-x}Si_xN$ films at RT: (a) $x = 0$; (b) $x = 0.04$; (c) $x = 0.08$; (d) $x = 0.11$.

is observed in the spectral range of 370–470 nm in the PL spectrum of AlN. However, a broad emission band centered at 402 nm is observed for 4% Si-doped AlN samples (Fig. 5b). When the Si doping content reaches 8% (Fig. 5c), the broad band comprises three emission peaks located at 404, 418, and 445 nm, respectively. And with further increase of Si content to 11% (Fig. 5d), it is obvious to note that the broad band contains a series of emission peaks located at 402, 416, 435, 447, and 465 nm, respectively. It is expected that these emission peaks could display the defects levels of Si-doped AlN films. According to the literature, the 402 nm emission band could be assigned to the native defects [23]. Nitrogen vacancy may be responsible for the 416–418 nm and 465 nm emission bands [24–26]. The emission bands centered at 435 nm and 447 nm are likely to be related to oxygen impurities [27,28]. Above all, the PL spectra undoubtedly demonstrate that the presence of large-scale defects in Si-doped AlN films. Of course, the exact PL mechanism of Si-doped AlN films needs further investigation.

3.5. Magnetic property analysis

Magnetization versus applied field M (H) data of $Al_{1-x}Si_xN$ ($x = 0$–0.11) films recorded at RT are shown in Fig. 6, where the magnetic field was applied in the surface plane. The diamagnetic contributions from the Si substrate to the total magnetization were subtracted. As can be seen in Fig. 6a, pure AlN films exhibit diamagnetic behaviors and no hysteresis behavior is observed. However, the ferromagnetic behavior has been observed for all Si doped AlN films. When $x = 0.04$, very weak ferromagnetism signals were detected, as shown in Fig. 6b. At higher doping concentrations of Si ($x \geq 0.08$), both the M–H curves are in the shape of a distinct hysteresis loop (Fig. 6c and d). The saturation magnetizations M_S are 2.01×10^{-6} and 3.13×10^{-6} emu for the films with $x = 0.08$ and 0.11, respectively, and the corresponding coercive fields H_c are 89 and 110 Oe (see inset of Fig. 6c and d). It is noteworthy that ferromagnetism signals of Si-doped AlN enhanced slightly with increasing Si content. To determine the T_c of the samples, the temperature dependence of the remnant magnetization (M_r) was measured.

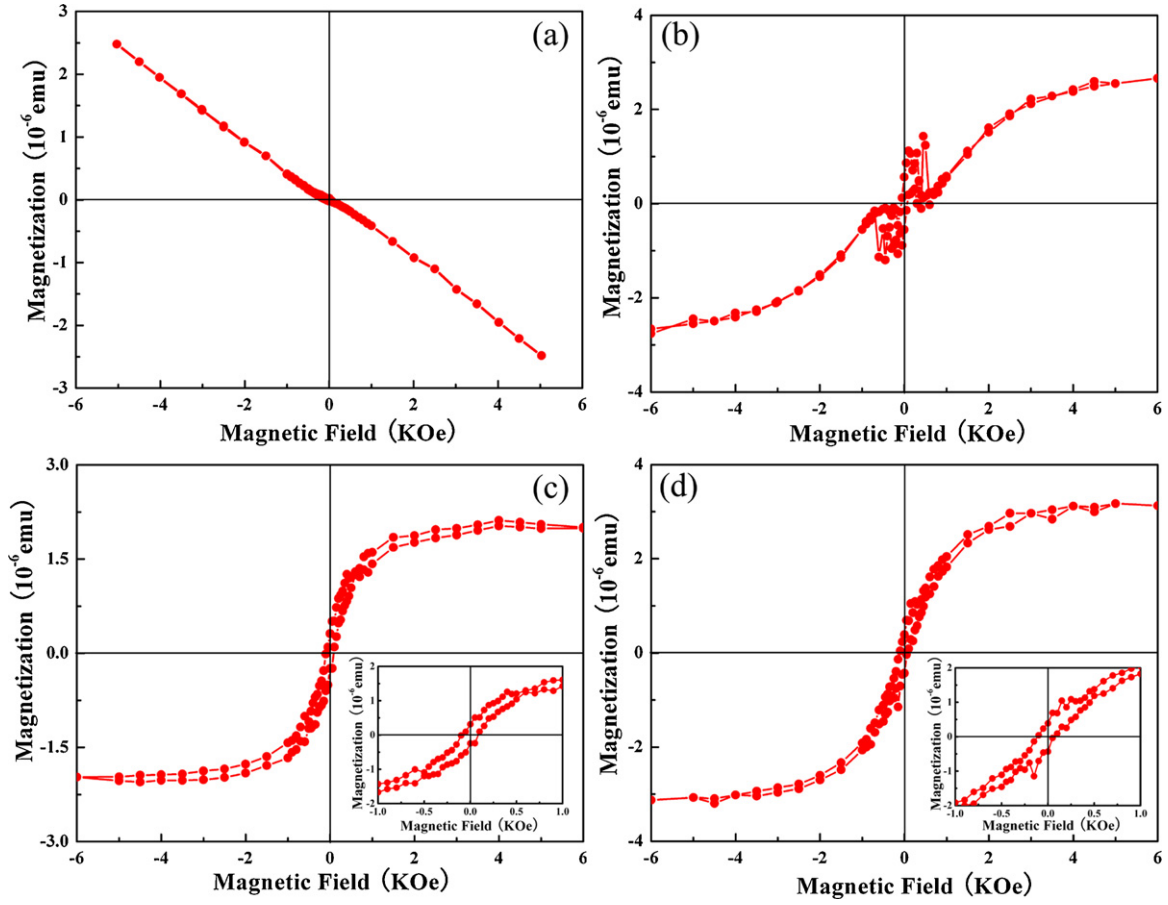

Fig. 6. Hysteresis loops for the $Al_{1-x}Si_xN$ films measured at RT: (a) $x = 0$; (b) $x = 0.04$; (c) $x = 0.08$; (d) $x = 0.11$. The insets in (c) and (d) are enlargement of the hysteresis loops.

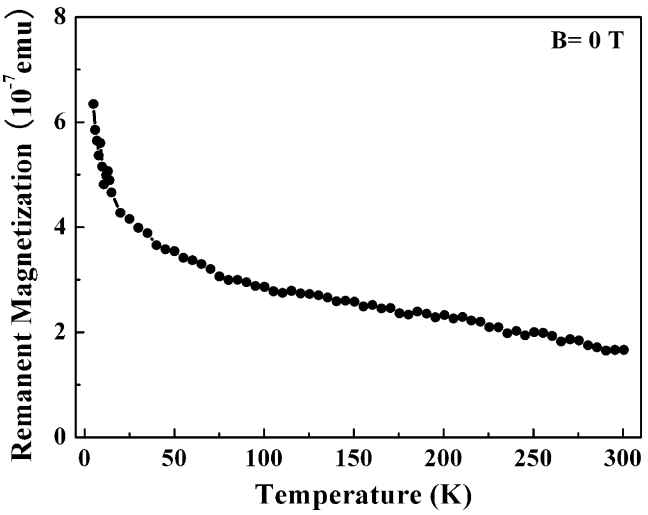

Fig. 7. Temperature dependence of remanent magnetization of 8% Si-doped AlN film.

Fig. 7 is a typical M_r–T curve of Si-doped AlN film with $x = 0.08$, which reveals the T_c of the deposited films is higher than 300 K.

To date, the origin of ferromagnetism order in nonmagnetic elements-doped AlN is less studied. For the natural ferromagnetism origin in Si-doped AlN, the possible impurity effects could be excluded since the starting materials of silicon do not exhibit long-range magnetic order features. The possible impurity magnetic phases from the contribution of magnetic phase can also be eliminated since all possible phases in the Al–Si–N ternary system are non-ferromagnetism. That is to say, the ferromagnetism order in this study must be intrinsic.

At present, there seems to be no single theoretical model which can explain the ferromagnetism in all DMS materials. Ferromagnetism based on free-carrier mediated models predicted for Mn-doped III–V semiconductors may not be applicable to AlN as it is highly resistive at RT. Recently, defects are found to play a great role in the ferromagnetic ordering of DMSs. For instance, it was found that the localized defect states in sp system may also lead local moments and exhibit collective magnetism [29]. Typically, ferromagnetic order in various carbon-based materials has been observed and detailed investigations showed that only intrinsic defects could take responsibility for the observed ferromagnetic order [30,31]. In addition, structural defects were also reported to be the possible origin of ferromagnetic order in some sp–d system such as HfO_2 and sp system such as SnO_2 [32,33]. Very recently, the defects, such the cation vacancies, etc. inducing intrinsic long-range magnetic order were also investigated in III–V nitrides such as GaN and AlN. Davies et al.' work suggested that gallium vacancies play an important role in ferromagnetic ordering in Gd- and Si-coimplanted GaN [34]. Wu et al. reported that Al vacancy in Mg-doped AlN lead to spin-polarized ground states [9]. Usually, it is very difficult to induce cation vacancies in semiconductors as compared to the anion vacancy, because the formation energy of cation vacancy in semiconductors is very high. However, there are many evidences showing that anion vacancy defects can also produce local magnetic moments in GaN and AlN. A recent calculation by Liu et al. and Li et al. indicated the introduction of nitride (N) vacancy is beneficial to stabilize the ferromagnetic configuration and enhance the ferromagnetism in Cr-doped GaN and AlN [35,36]. Ferromagnetism due to create N vacancy was also reported in Cr and Cu-doped AlN films [12,37]. Based on PL and SQUID measurements, in our study, magnetic properties of Si-doped AlN films were improved when large-scale defects appeared in AlN lattice. Especially, the emission band arising from N vacancy in AlN lattice was observed for 8% Si-doping content, and this band is intensified when Si concentration is raised to 11%. This indicates heavy Si doping lead to a further increase of N vacancy. Note that increasing the N vacancy results in an obvious increase in the magnetization response, as seen above. Thus, we consider N vacancy should be responsible for the long-range magnetic order in Si-doped AlN films. The so-called bound magnetic polaron (BMP) models [38] may be applicable to the AlN:Si, in which the role of N vacancies in AlN:Si is similar to that of the oxygen vacancies in oxides. The N vacancies trap electrons and form F centers, as described in Ref. [37].

As reported by Fan et al. and Malindretos et al., oxygen point defects including O_N (O substituting for N) and O_i (isolated O interstitials) in Ti-doped AlN [10] and Gd-doped GaN [39] could induce intrinsic ferromagnetic order. The element O is the most common unintentional dopants in III–V semiconductors. In our work, emission peaks which are related with O impurities appeared in Si-doped AlN film with 8% and 11% Si doping. Thus, the effect of oxygen point defects on the ferromagnetism of Si-doped AlN films should also be considered. However, more investigations are necessary to indubitably identify the role of oxygen and the magnetic coupling mechanism in this material.

4. Conclusions

In summary, Si-doped AlN films with different Si dopings have been deposited on Si (1 0 0) substrates by radio frequency reactive sputtering. Si atoms were successfully incorporated into AlN, while the AlN crystal structure was maintained. All the doped samples exhibited ferromagnetism at RT and the maximum M_s and H_c obtained at 300 K were about 3.13×10^{-6} emu and 110 Oe, respectively. We deduce the defects such N vacancies have great contribution for ferromagnetism order in Si-doped AlN. It is expected that our findings may impact the spintronic research field due to its potential applications in magneto-electrical devices operating at RT. Thus, Si is a promising nonmagnetic dopant for AlN.

Acknowledgments

The authors are grateful to Professor J.H. Zhao for the help with magnetic measurements. This work was supported by Natural Science Foundation of China (Grant Nos. 10864004, 50862008, 11164026, 51172793), and The China Postdoctoral Science Foundation funded project (Grant Nos. 20100471679, 201104704). The authors also thank the open fund of Surface Physics Laboratory (National Key Laboratory), Fudan University, China.

References

[1] S.A. Wolf, D.D. Awschalom, R.A. Buhrman, J.M. Daughton, S. von Molnár, M.L. Roukes, A.Y. Chtchelkanova, D.M. Treger, Science 294 (2001) 1488–1495.
[2] D. Kumar, J. Antifakos, M.G. Blamire, Z.H. Barber, Appl. Phys. Lett. 84 (2004) 5004–5006.
[3] Y. Endo, T. Sato, A. Takita, Y. Kawamura, M. Yamamoto, IEEE Trans. Magn. 41 (2005) 2718–2720.
[4] H.X. Liu, S.Y. Wu, R.K. Singh, L. Gu, D.J. Smith, N. Newman, N.R. Dilley, L. Montes, M.B. Simmonds, Appl. Phys. Lett. 85 (2004) 4076–4078.
[5] M.H. Ham, S. Yoon, Y. Park, J.M. Myoung, J. Cryst. Growth 271 (2004) 420–424.
[6] X.H. Ji, S.P. Lau, S.F. Yu, H.Y. Yang, T.S. Herng, A. Sedhain, J.Y. Lin, H.X. Jiang, K.S. Teng, J.S. Chen, Appl. Phys. Lett. 90 (2007) 193118–193120.
[7] S.L. Yang, R.S. Gao, P.L. Niu, R.H. Yu, Appl. Phys. A 96 (2009) 769–774.
[8] H. Li, H.Q. Bao, B. Song, W.J. Wang, X.L. Chen, Solid State Commun. 148 (2008) 406–409.
[9] R.Q. Wu, G.W. Peng, L. Liu, Y.P. Feng, Z.G. Huang, Q.Y. Wu, Appl. Phys. Lett. 89 (2006) 142501–142503.
[10] S.W. Fan, K.L. Yao, Z.G. Huang, J. Zhang, G.Y. Gao, G.H. Du, Chem. Phys. Lett. 482 (2009) 62–65.
[11] K. Li, X.B. Du, Y. Yan, H.X. Wang, Q. Zhan, H.M. Jin, Phys. Lett. A 374 (2010) 3671–3675.
[12] F.Y. Ran, M. Subramanian, M. Tanemura, Y. Hayashi, T. Hihara, Appl. Phys. Lett. 95 (2009) 112111–112113.

[13] W.W. Lei, D. Liu, P.W. Zhu, X.H. Chen, Q. Zhao, G.H. Wen, Q.L. Cui, G.T. Zou, Appl. Phys. Lett. 95 (2009) 162501–162503.
[14] M. Khizar, Z.Y. Fan, K.H. Kim, J.Y. Lin, H.X. Jiang, Appl. Phys. Lett. 86 (2005) 173504–173506.
[15] M. Hermann, F. Furtmayr, F.M. Morales, O. Ambacher, M. Stutzmann, M. Eickhoff, J. Appl. Phys. 100 (2006) 113531–113540.
[16] M. Kasu, Y. Taniyasu, N. Kobayashi, Jpn. J. Appl. Phys. Part 2 40 (2001) L1048–L1050.
[17] C.D. Wagner, W.M. Riggs, L.E. Davis, J.F. Moulder, Handbook of X-ray Photoelectron Spectroscopy, Physical Electronics Division, Perkin-Elmer, 1979, pp. 51–53.
[18] S.Y. Ren, W.Y. Ching, Phys. Rev. B 23 (1981) 5454–5463.
[19] F.A. Ponce, C.G.V. Walle, J.E. Northrup, Phys. Rev. B 53 (1996) 7473–7478.
[20] R. Frazier, G. Thaler, M. Overberg, B. Gila, C.R. Abernathy, S.J. Pearton, Appl. Phys. Lett. 83 (2003) 1758–1760.
[21] M. Kasu, N. Kobayashi, Appl. Phys. Lett. 78 (2001) 1835–1837.
[22] Y. Taniyasu, M. Kasu, T. Makimoto, Appl. Phys. Lett. 84 (2004) 2115–2117.
[23] Y.W. Ma, K.F. Huo, Q. Wu, Y.N. Lu, Y.M. Hu, Z. Hu, Y. Chen, J. Mater. Chem. 16 (2006) 2834–2838.
[24] H.T. Chen, X.L. Wu, X. Xiong, W.C. Zhang, L.L. Xu, J. Zhu, P.K. Chu, J. Phys. D: Appl. Phys. 41 (2008) 025101–025106.
[25] Y.G. Cao, X.L. Chen, Y.C. Lan, J.Y. Li, Y.P. Xu, T. Xu, Q.L. Liu, J.K. Liang, J. Cryst. Growth 213 (2000) 198–202.
[26] R.A. Youngman, J.H. Harris, D.A. Chernoff, Ceram. Trans. 5 (1989) 309–314.
[27] C.K. Xu, L. Xue, C.R. Yin, G.H. Wan, Phys. Status Solidi A 198 (2003) 329–335.
[28] Y.C. Lan, X.L. Chen, Y.G. Cao, Y.P. Xu, L.D. Xun, T. Xu, J.K. Liang, J. Cryst. Growth 207 (1999) 247–250.
[29] A.L. Rosa, R. Ahuja, Appl. Phys. Lett. 91 (2007) 232109–232111.
[30] Y. Zhang, S. Talapatra, S. Kar, R. Vajtai, S.K. Nayak, P.M. Ajayan, Phys. Rev. Lett. 99 (2007) 107201–107205.
[31] T.L. Makarova, B. Sundqvist, R. Höhne, P. Esquinazi, Y. Kopelevich, P. Scharff, V.A. Davydov, L.S. Kashevarova, A.V. Rakhmanina, Nature 413 (2001) 716–718.
[32] E. Tirosh, G. Markovich, Adv. Mater. 19 (2007) 2608–2612.
[33] N.H. Hong, N. Poirot, J. Sakai, Phys. Rev. B 77 (2008) 033205–033209.
[34] R.P. Davies, B.P. Gila, C.R. Abernathy, S.J. Pearton, C.J. Stanton, Appl. Phys. Lett. 96 (2010) 212502–212504.
[35] Y.L. Li, W.L. Fan, H.G. Sun, X.F. Cheng, P. Li, X. Zhao, M.H. Jiang, J. Solid State Chem. 183 (2010) 2662–2668.
[36] L.J. Shi, L.F. Zhu, Y.H. Zhao, B.G. Liu, Phys. Rev. B 78 (2008) 195206–195214.
[37] J. Zhang, X.Z. Li, B. Xu, D.J. Sellmyer, Appl. Phys. Lett. 86 (2005) 212504–212506.
[38] J.M.D. Coey, A.P. Douvalis, C.B. Fitzgerald, M. Venkatesan, Appl. Phys. Lett. 84 (2004) 1332–1334.
[39] M. Roever, J. Malindretos, A.B. Pinto, A. Rizzi, Phys. Rev. B 84 (2011) 081201–081205.